Songklanakarin J. Sci. Technol.
44 (1), 157-161, Jan. - Feb. 2022

http://www.sjst.psu.ac.th

Original Article

Numerical simulations of single whispering-gallery mode enhancement in hollow cylindrical optical microcavity

Unchittha Prasatsap[1], and Suwit Kiravittaya[1, 2*]

[1] *Advanced Optical Technology Laboratory, Department of Electrical and Computer Engineering, Faculty of Engineering, Naresuan University, Mueang, Phitsanulok, 65000 Thailand*

[2] *Semiconductor Device Research Laboratory, Department of Electrical Engineering, Faculty of Engineering, Chulalongkorn University, Pathum Wan, Bangkok, 10330 Thailand*

Received: 31 August 2020; Revised: 8 March 2021; Accepted: 28 April 2021

Abstract

In this work, a hollow cylindrical optical microcavity is numerically investigated by finite-difference time-domain simulations. Enhancement of a single whispering-gallery mode (WGM) is realized by inserting a periodic hole array into the hollow cylindrical structure. Line of missing holes acts as an optical microcavity. Electric and magnetic field profiles of both typical and enhanced resonant modes are presented. Variations of the single-mode resonant frequency and its quality (*Q*) factor are studied as a function of structural parameters, which are hole radius, width of the missing hole line, and number of holes. This work shows that the hole radius and the width of the missing hole line strongly affect both the resonant frequency and *Q* factor while varying the number of holes does not influence the resonant frequency, but they monotonically change the *Q* factor. This work provides information for designing and optimizing an WGM optical microcavity.

Keywords: whispering-gallery mode, optical microcavity**,** finite-difference time-domain simulation, hollow cylinder**,** quality factor

1. Introduction

Structured materials that can control light in single photon level are important systems for the development of novel photonic quantum materials and technologies (Joannopoulos, Johnson, Winn & Meade, 2008; Ozawa *et al.*, 2019; Song, 2019). Realization of single as well as entangled photon sources has intensively been investigated in the last decade (Lodahl, Mahmoodian & Stobbe, 2015; Orieux, Versteegh, Jöns & Ducci, 2017). Among the explored systems, whispering-gallery mode (WGM) optical microcavities are a promising structure due to their intrinsic high quality (*Q*) factor. Several photonic devices based on this kind of microcavity have been commercialized. However, typical WGM microcavities, such as microdisks, microrings, and microtubes, confine many optical modes, which are grouped into sets and labeled by different indices. For single mode operation, a way to select one single active mode is highly desired. Recently, we have presented the experimental realization of selected and enhanced single WGM emission by utilizing patterned hole array (Tian *et al.*, 2018). Thin diamond membrane is self-rolled to form a microtube cavity. By pre-defining the number of patterned holes along the circumference, a single well-defined WGM mode can be enhanced while other modes are suppressed, as has been observed in photoluminescence spectroscopy experimentally. However, an investigation on the sensitivity of the optical mode for each structural parameter is still missing.

In this work, numerical simulations of the single WGM enhancement in hollow cylindrical optical microcavities will be described. To complement the finite element approach and coupled-wave theory presented in Ref. (Tian *et al.* 2018) and its Supporting Information, finite-difference time-domain (FDTD) simulation is applied in this

*Corresponding author
Email address: suwitki@gmail.com; suwit.ki@chula.ac.th

work. The results extracted from these temporal simulations will be presented and discussed. Since structural parameters of the microcavity can easily be varied in the simulation, we can utilize this approach to engineer the material and structure prior to any experimental realization.

2. Simulation Procedure

Firstly, three-dimensional (3D) tubular structure is simplified to a planar (2D) domain as shown in Figure 1. This means that the propagation directions and corresponding wave fields become in-plane and radiative loss is neglected. The latter is justified in both high-refractive-index and small-curvature optical microcavities. Selection of the material parameters has been done according to the experimental work (Tian *et al.*, 2018). They are refractive indices of microcavity and air holes. For this reduced dimensional system (from 3D to 2D), the index of cavity can be presented by an effective index and we set it to 2.0. Index of air is set to 1.0. Tube diameter (D in Figure 1(a)) transforms to lateral distance L, which equals the product of number of holes N along x-direction and hole period a (Figure 1(b)). Investigated structural parameters are the hole radius r, the width of the missing hole line w, the number of hole columns N along x-direction and the number of hole rows M along y-direction. Periodic boundary is set for confining the propagating waves in the cavity while absorbing boundary is set for escaping waves. Note that a small domain size compared with the reference (Tian *et al.*, 2018) is considered in this work. However, both this work and the reference show the confined WGM mode with the azimuthal mode index m around the number of hole columns N ($m \approx N$).

Simulations are performed with the FDTD method (Taflove & Hagness, 2005), using an open-source software package named MEEP (Oskooi *et al.*, 2010). Normalized units are used throughout this work (Joannopoulos, Johnson, Winn & Meade, 2008). The hole period a and the characteristic frequency unit of c/a ($c = 3\times10^8$ m/s) are the natural length and frequency scale. Typical hole period is 320–400 nm and typical resonant wavelength is in visible and near-IR ranges (Tian *et al.*, 2018). Figures 2(a) and 3(a) show schematics of the investigated symmetric and asymmetric simulation domains. A perfectly matched layer (PML) of thickness a is applied as the absorbing boundary condition for escaping waves, while the periodic boundary condition is set for the confined waves. Simulation resolution is fixed at $a/32$ while typical structural parameters are $r = 0.25a$, $w = a$, $N = 20$, and $M = 3$. The H_z dipole source and monitoring point are marked with crosses in Figures 2(a) and 3(a). Only the modes with perpendicular magnetic field H_z (and in-plane electric fields, E_x and E_y) are considered since the hollow cavity with thin wall usually supports only this polarized mode (Hosoda & Shigaki, 2007). A Gaussian pulse at single frequency (at about resonant frequency f_c) with narrow frequency band ($\Delta f = 0.01$ (c/a)) is used to excite the optical field. After the pulse decays, the field profiles are recorded and the simulation is ended. Harmonic inversion routine implemented in MEEP is used to extract the resonant frequency f_c and the Q factor ($= -\omega_r/2\omega_i$, where ω_r and ω_i are real and imaginary parts of the complex resonance frequency, which is obtained by performing the Fourier transform of the time domain signal (Joannopoulos, Johnson, Winn & Meade, 2008)). With the described procedure, unambiguous single resonant frequency f_c and Q factor are usually obtained. The Q factor physically represents the ability to confine light within the structure at the specific mode index m.

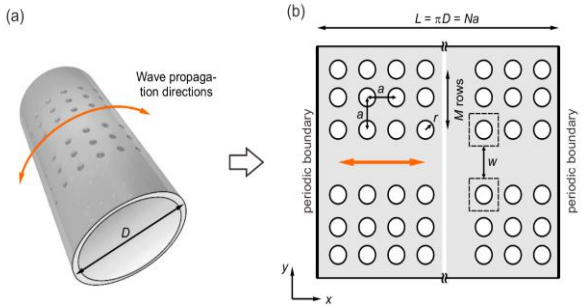

Figure 1. (a) 3D schematic of the investigated hollow cylindrical optical microcavity and (b) the simplified 2D structure. Arrows in both figures are the considered wave propagation directions. In (b), the unit cells of square hole array have the size $a \times a$ and are marked with dashed squares. Investigated parameters are the hole radius r, the width of missing hole line w, and the numbers of holes N along x-direction and M along y-direction.

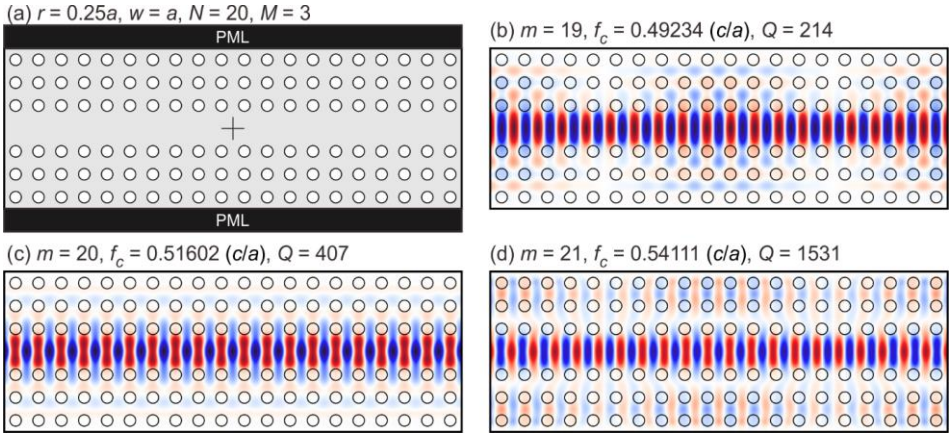

Figure 2. (a) Simulation domain for low Q modes. The H_z dipole source and monitoring point are marked with crosses. (b–d) Extracted resonant magnetic field profiles H_z for m = (b) 19, (c) 20, and (d) 21. Values of resonant frequency f_c and Q factor are shown.

3. Results and Discussion

3.1 Mode profiles

Figures 2(b), 2(c), and 2(d) respectively show the resonant mode fields for the mode indexes m = 19, 20, and 21 obtained from the simulations with the symmetric domain shown in Figure 2(a). These modes have typical resonant frequencies f_c, which can be calculated from $f_c = m/nN$, where n is the effective index. This relation is equivalent to the well-known $L = m\lambda/n$, where λ is the optical wavelength in vacuum. Similar to other microcavities, optical leakage of each mode can be characterized by its Q factor but this microcavity does not show a clear trend of the Q factor variation as a function of mode index m, unlike typical WGM cavities such as microdisks (Xu, Lee & Yariv, 2000). We attribute this to the variation of spatial mode field interaction with the patterned holes. Since the matching of the hole period and the field wavelength occurs only at $m = N$, the other modes will experience a different scattering loss at the hole edge. For the case $m = N$ (= 20 in this simulation), lossy field profile ($Q \sim 407$) is obtained because of the large overlap between the magnetic field H_z and the patterned holes.

Figure 3 shows the simulation domain and the simulation results related to the enhanced WGM mode at $m = N = 20$. In Figure 3(a), the asymmetric simulation domain is shown. For this simulation, the whole hole array is shifted by $0.25a$ in x-direction while other parameters are unaltered. This shift is similar to the simultaneous changes of the excitation source and the boundary location and it results in the appearance of an enhanced single mode. Figures 3(b), 3(c), and 3(d) show the magnetic and electric field profiles, H_z, E_x, and E_y, of the enhanced mode, respectively. These fields can perfectly be related to each other by Maxwell's equations (Joannopoulos, Johnson, Winn & Meade, 2008; Taflove & Hagness, 2005). Based on the obtained electric and magnetic fields, the electric and magnetic field energy densities can be calculated and they are shown in Figs. 3(e) and 3(f). In this time domain simulation, one can observe temporal oscillations of these field energies. Note, that this electric energy density profile (Figure 3(e)) is qualitatively similar to the field profile shown in Ref. (Tian *et al.*, 2018). Since the calculations shown in Ref. (Tian *et al.*, 2018) are done with the finite element method and are supported by the coupled-wave theory (Kogelnik & Shank, 1972), we are confident that the results from our FDTD simulation are correct and consistent with other calculation approaches.

3.2 Effects of structural parameters

Starting with the typical parameter set and the obtained mode profiles (Figure 3), one can further investigate the enhanced WGM properties. In all cases shown below, the simulated profiles look rather similar to the one shown in Figure 3. We thus do not show and discuss the spatial profile; only values of the resonant frequency f_c and Q factor are summarized.

Figure 4(a) shows the variation of the resonant frequency f_c and the Q factor as functions of hole radius r. When the radius increases, the resonant frequency blueshifts. The extracted positive slope of this relation is $(0.05305 \pm 1.93 \times 10^{-4})c$ and can be explained by (1) the narrowing of the effective width of the field as well as (2) the decrease in effective index of the hole array. Since enlarging the holes reduces the waveguiding area, this is similar to decreasing the width w of the missing hole line (Figure 4(b) and the discussion below).

Moreover, from viewpoint of the effective index, one might consider increasing the hole radius to lower the effective index, and this results in a blueshift in the resonant frequency. An analogy to the electron eigenenergy in a finite square well in Quantum Mechanics can be made here (Davies,

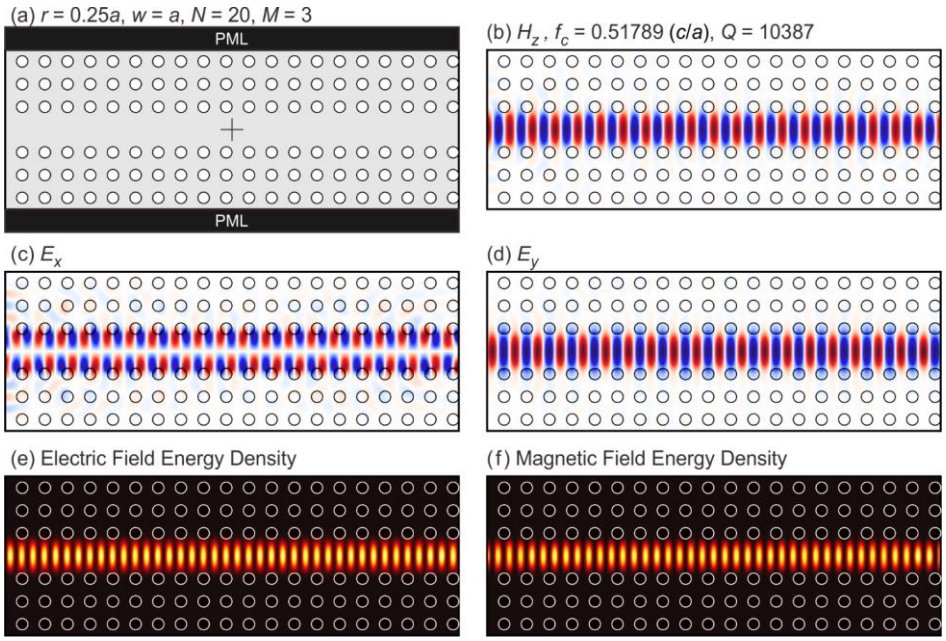

Figure 3. (a) Simulation domain for single high Q mode. The H_z dipole source and monitoring point are marked with crosses. (b–f) Extracted resonant profiles for m = 20 of (b) H_z, (c) E_x, (d) E_y, and (e) electric and (f) magnetic field energy densities.

1998; Griffiths, 2014). The electron confinement energy is higher when the barrier height increases (Figure 4(a)). Moreover, this energy can be lowered by increasing the well width (Figure 4(b)).

Interestingly, the Q factor can be locally optimized by changing the hole radius r. A high Q value of 10387 is obtained when the hole radius is set to $0.21a$. This might be due to the optimum configuration for interaction between the field profile and the spatial index variation. Further Q factor optimization might be done by simultaneously changing several parameters. However, it is not in the scope of this work.

Figure 4(b) shows the variation of the resonant frequency f_c and the Q factor as functions of width of missing hole line w. When the width increases, the resonant frequency redshifts. The extracted negative slope of this relation is $(-0.01978 \pm 2.33\times10^{-4})c$ and can be explained by the widening of the field width. For the Q factor variation, we find that the Q factor monotonically increases with the width w. Further enhancement of the Q factor might be achieved by further varying this parameter. However, appearance of higher order modes along the y-direction and narrowing of the mode spacing might have to be considered.

Figure 5(a) shows the variation of the resonant frequency f_c and the Q factor as functions of hole number N along x-direction. This parameter is the number of hole columns and it is equivalent to the microcavity diameter D (Figure 1(b)). When the number of columns increases, the resonant frequency remains constant and the observed variation is from numerical uncertainty. This result is correct according to the theory (Tian *et al.*, 2018). However, we further observe an increase in Q factor with the number of hole columns N. A high Q factor of 18097 is observed when N is set at 40 and it seems that the value can be further increased by simulating in a larger domain. This might be explained by the better dynamic adjustment of field profile in a larger confined structure.

Figure 5(b) shows the variation of the resonant frequency f_c and the Q factor as functions of hole number M along y-direction. Since this number of rows indicates the level of lateral confinement similar to an electron in quantum well, we can view it as the barrier layer and the $M = 1$ case is the lower limit. According to our FDTD simulations, the obtained resonant frequency f_c is constant (within the numerical uncertainty) while the Q factor monotonically increases with the number of rows M. A low Q value of 3896 is observed for $M = 1$ while a high Q value of 14607 is achieved with five rows of holes ($M = 5$) implemented in the simulation. Further enhancement of the Q value might be possible with this parameter. However, the realization of hollow cylindrical microcavity by self-rolling process might be influenced by a change in the number of holes since intrinsic strain might be decreased in nanomembranes with a large number of patterned holes. In addition, the presence of inner and outer notches in the rolled-up structure inevitably breaks the system symmetry and thus degrades the Q value.

4. Conclusions

We have described FDTD simulations of hollow cylindrical optical microcavity by first transforming the structure and then setting up the simulation domains. In our simulations, a symmetric domain is used for simulating typical (low Q) modes. The high Q mode is obtained when an asymmetric domain is considered. All relevant profiles are presented and discussed. The resonant frequency of high-Q

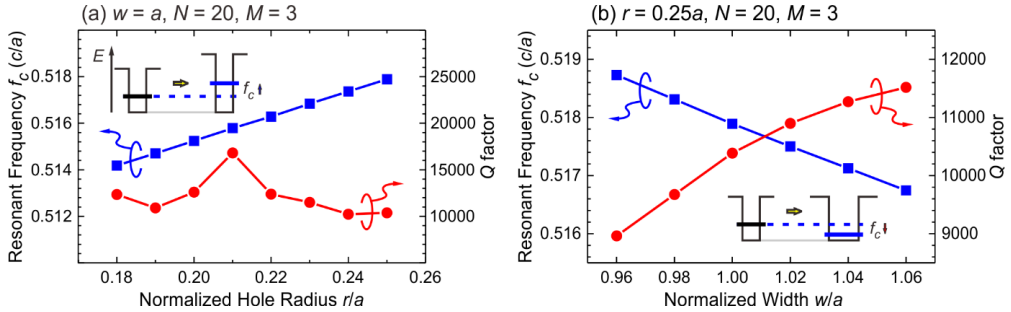

Figure 4. Variations of resonant frequency and Q factor as functions of (a) hole radius r and (b) width of missing hole line w. Insets in both figures show the analogies between quantum mechanical finite square well and the investigated system.

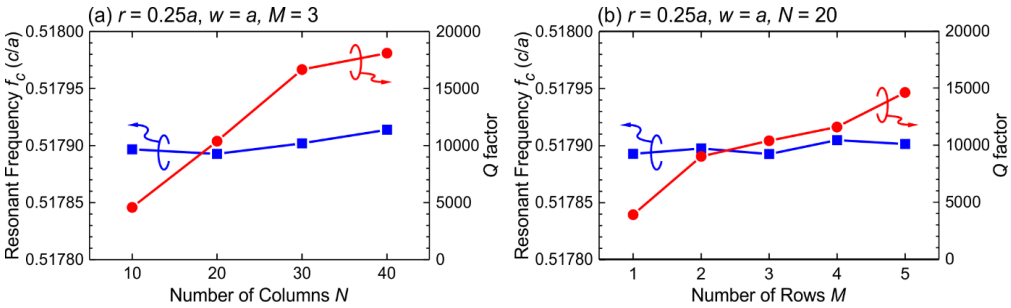

Figure 5. Variations of resonant frequency and Q factor as functions of numbers of (a) hole columns in x-direction N and (b) hole rows in y-direction M.

mode shows linear variations with the patterned hole radius and the width of the missing hole line, while the *Q* factor depends on all investigated parameters (hole radius, width, and numbers of holes in both vertical and horizontal directions). These simulations provide useful information as a basis for design and optimization of a single-mode optical microcavity.

Acknowledgements

This research is financially supported by Thailand Research Fund (TRF) through the Royal Golden Jubilee Ph.D. program (contract no. PHD/0078/2561) and the Fudan Fellow scholarship. The Research Chair Grant of the National Science and Technology Development Agency (NSTDA), Thailand (Contract No. FDA-CO-2558-1407-TH) and the group of Prof. Somsak Panyakeow at the Semiconductor Device Research Laboratory (SDRL), Department of Electrical Engineering, Faculty of Engineering, Chulalongkorn University are also acknowledged. The authors thank the long-term collaboration and friendship with Prof. Yongfeng Mei.

References

Davies, J. H. (1998). *Physics of low-dimensional semiconductors: an introduction*. New York, NY: Cambridge University Press.

Griffiths, D. J. (2014). *Introduction to quantum mechanics* (2nd ed.). Essex, England: Pearson.

Hosoda, M. & Shigaki, T. (2007). Degeneracy breaking of optical resonance modes in rolled-up spiral microtubes. *Applied Physics Letters*, *90*(18), 687–702. doi: 10.1063/1.2734878

Joannopoulos, J. D., Johnson, S. G., Winn, J. N. & Meade, R. D. (2008). Photonic crystals: molding the flow of light (2nd ed.). Princeton, NJ: Princeton University Press.

Kogelnik, H. & Shank, C. V. (1972). Coupled-wave theory of distributed feedback lasers. *Journal of Applied Physics*, *43*(5), 2327–2335. doi:10.1063/1.1661499

Lodahl, P. Mahmoodian, S. & Stobbe, S. (2015). Interfacing single photons and single quantum dots with photonic nanostructures. *Reviews of Modern Physics*, *87*(2), 347-400. doi:10.1103/RevModPhys.87.347.

Orieux, A., Versteegh, M. A. M., Jöns, K. D. & Ducci, S. (2017). Semiconductor devices for entangled photon pair generation: A review. *Reports on Progress in Physics*, *80*(7), 1-29. doi:10.1088/1361-6633/aa6955

Oskooi, A., Roundy, D., Ibanescu, M., Bermel, P., Joannopoulos, J. D. & Johnson, S. G. (2010). Meep: A flexible free-software package for electro magnetic simulations by the FDTD method. *Computer Physics Communications*, *181*(3), 687–702. doi:10.1016/j.cpc.2009.11.008

Ozawa, T., Price, H. M., Amo, A., Goldman, N., Hafezi, M., Lu, L., . . . Carusotto, I. (2019). Topological photonics. *Reviews of Modern Physics*, *91*(1), 1-76. doi: 10.1103/RevModPhys.91.015006

Song, Q. (2019). Emerging opportunities for ultra-high Q whispering gallery mode microcavities. *Science China Physics, Mechanics and Astronomy*, *62*(7), 1-4. doi:10.1007/s11433-018-9349-2

Taflove, A. & Hagness, S. C. (2005). Computational electrodynamics: The finite-difference time-domain method. Norwood, MA: Artech.

Tian, Z., Li, S., Kiravittaya, S., Xu, B., Tang, S., Zhen, H., . . . Mei, Y. (2018). Selected and enhanced single whispering-gallery mode emission from a mesostructured nanomembrane microcavity. *Nano Letters*, *18*(12), 8035-8040. doi:10.1021/acs.nanolett.8b04259

Xu, Y., Lee, R. K. & Yariv, A. (2000). Finite-difference time-domain analysis of spontaneous emission in a microdisk cavity. *Physical Review A*, *61*, 1–10. doi:10.1103/PhysRevA.61.033808